Electronic Supplementary Information

(ESI)for the article:

"On the Opto-electronic Properties of Phosphine and Thiolate-protected Undecagold Nanoclusters"

Francesco Muniz-Miranda,* Maria Cristina Menziani, and Alfonso Pedone*

University of Modena and Reggio Emilia, Department of Chemical and Geological Sciences, Via G. Campi 183, 41125, Modena, Italy

E-mail: francesco.munizmiranda@unimore.it; alfonso.pedone@unimore.it

*To whom correspondence should be addressed

XC Functionals on NC1 GIC Model

Time-dependent density functional calculations on the Gold-Inner-Core of $Au_{11}(PPh_3)_7Cl_3$ with one explicit ligand molecule (**GIC+L** model in Figure 1 of the paper) have been carried out by employing the range-separated cam-B3LYP, the B3LYP and M06-HF hybrids, and the GGA B-PBE exchange-correlation (XC) functionals. For the $Au_{11}(PPh_3)_7Cl_3$ (NC1) and $Au_{11}(PPh_3)_7SPyr_3$ (NC2) nanoclusters these four XC functionals yielded fairly accurate structures.[1] The electronic spectra of the NC1 **GIC+L** model computed with these four functionals are reported in Fig. S1. The whole spectra (blue lines) have been obtained by convolving 100 $S_0 \rightarrow S_n$ transitions (red sticks in Fig. S1) with Gaussians of half-width at half height of 0.25 eV. No shift of the wavelengths was applied in this case. The results of calculations with cam-B3LYP, B3LYP, and M06-HF yield a very similar shape for the UV-Vis spectrum, with two very recognizable absorption bands separated of about 90 nm, in excellent agreement with the experimental value of 88 nm.

The shallow minimum at about 360 nm in the B3LYP-calculated spectrum could be considered an artifact of the convolution procedure: reducing slightly the half-width of the Gaussian functions (*e.g.* to 0.2 eV), a shape very similar to those given by cam-B3LYP and M06-HF can be obtained. Also the transitions, approximated by the red spikes, appear quite similar for these three functionals. B3LYP yields the λ_{max} closer to the experimental values (316 and 406 nm), while cam-B3LYP-calculated wavelengths should be translated by a factor of about +50 nm for a better comparison with the UV-Vis experimental spectrum. The translating factor for M06-HF is greater than this ($\sim$100 nm).

The spectrum obtained employing the B-PBE XC functional shows a different general shape (blue line) and energetics (red spikes). While transitions calculated with cam-B3LYP/B3LYP/M06-HF functionals are clustered around two regions, those given by B-PBE appear spread in a wide range of wavelengths and the two characteristic peaks separated by $\sim$90 nm do not occur. However, the $S_0 \rightarrow S_1$ transition

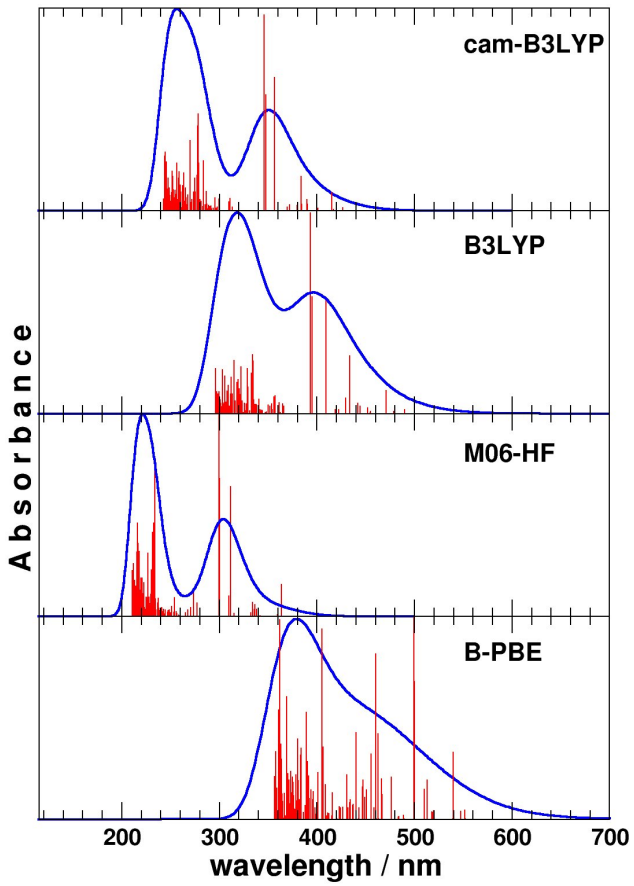

Figure S1: UV-Vis spectra (blue lines) of the NC1 **GIC+L** model obtained from the convolution of 100 $S_0 \rightarrow S_n$ transitions (red sticks) with Gaussians of half-width at half-height of 0.25 eV. Wavelengths have not been shifted.

(the so-called "optical-gap"[2]) is in agreement with the experimental-extrapolated one within ∼0.1 eV margin of error.[3] As was expected from theoretical considerations,[2] this result was found with previous calculations employing a more limited basis set for the organic ligands.[1]

Choice of Basis-Sets for PPh_3

In order to find the best compromise between accuracy and computational burden in the calculation of electronic spectrum of the full nanoclusters, a benchmarking of various basis sets has been carried out for triphenylphosphine, ligand to both NC1 and NC2. Figure S2 displays the TD-DFT calculated optical spectra (computed by using

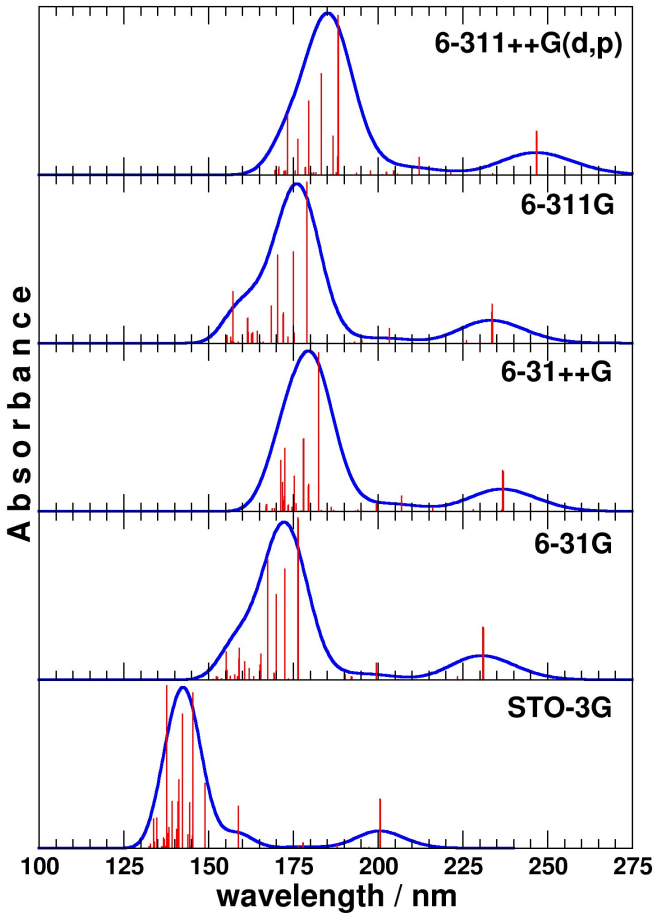

Figure S2: TD-DFT spectra of triphenylphosphine. 50 $S_0 \rightarrow S_n$ transitions have been taken into account. cam-B3LYP XC functional has been employed. Blue lines and red spikes denote spectra obtained by convolving the first 50 $S_0 \rightarrow S_n$ transitions with Gaussians of half-width at half-height of 0.25 eV. Wavelengths have not been shifted.

50 $S_0 \rightarrow S_n$ transitions) of PPh_3 using cam-B3LYP and 5 different basis sets, namely STO-3G, 6-31G, 6-31++G, 6-311G and 6-311++G(d,p). Calculations have been performed on the optimized structure of PPh_3 at the cam-B3LYP/6-311++G(d,p) level of theory. The spectrum obtained with 6-311++G(d,p) basis sets can be regarded as the reference calculation, at least for the purposes of the present benchmarking.

As can be seen, both triple-zeta 6-311G and double-zeta 6-31G basis sets yield a distorted shape of the spectrum, with a clear shoulder at shorter wavelengths that is absent in the spectrum obtained with the reference basis set. Transitions provided by STO-3G calculations, the simplest basis-set tested here, are very blue-shifted, and the

shape of the spectrum is narrower than reference calculation. It has to be pinpointed that in previous full-DFT calculations[1] on NC1 and NC2, 6-31G and STO-3G basis sets have been employed to investigate the structural accuracy of the DFT approach and to recover the optical gap (*i.e.* the $S_0 \rightarrow S_1$ transition energy).

Calculations performed by using the 6-31++G basis sets yield the spectrum in better agreement with the reference spectrum. The possible addition of polarization functions to this latter double-zeta basis sets (attempted but not reported) does not significantly improve the optical spectrum (only a very slight red-shift of the energies is observed), but severely hinders the feasibility of TD-DFT calculations on the complete $Au_{11}(PPh_3)_7Cl_3$ nanocluster. Thus, addition of two diffuse functions to the 6-31G basis-set seems to be preferred to adding polarization functions, and for this reason the 6-31++G basis-set has been adopted for the organic ligands in the computation reported in the main article. However, Cl and P atoms have been treated with a 6-31++G(d,p) basis-set to account for the hypervalence state of the latter. The main contribution to the first band of the UV-Vis spectrum of PPh_3 at the cam-B3LYP/6-31++G level of theory is given by the transition between the HOMO and LUMO+1 Kohn-Sham molecular orbitals displayed in Figure S3.

Excited States of the NC1 GIC+L Model

The most significant $S_0 \rightarrow S_n$ transitions of the **GIC+L** model of NC1 (computed with cam-B3LYP functional) are reported in Table S1. Only transitions whose oscillator strength is greater than 0.0250 are reported there, with exception of excited states $\boldsymbol{n}$=1 and 144, for their relevance. The occupied and virtual orbitals contributing to these transitions are reported as well, along the coefficient of the contribution (4^{th}column). Most of the orbitals cited in Table 1 are also pictured in Figures S4 and S5 as contour levels. As can be appreciated, **GIC**$\rightarrow$**GIC** transitions are ubiqui-

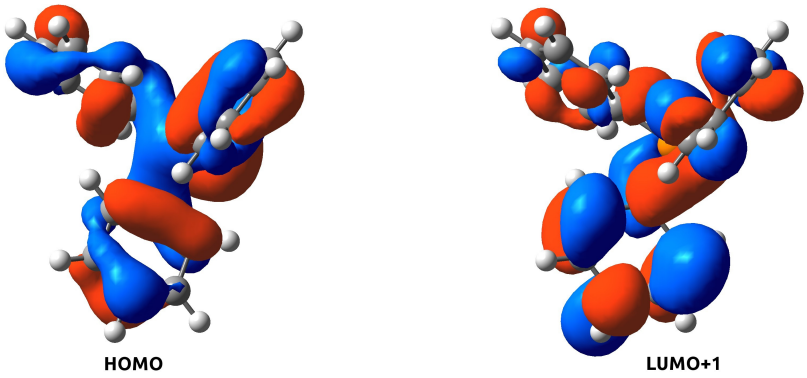

Figure S3: Contour levels for HOMO and LUMO+1 of triphenylphosphine at cam-B3LYP/6-31++G level of theory. These orbitals give the main contribution to the $S_0 \rightarrow S_1$ transition of 5.23 eV (corresponding to λ =237 nm, oscillator strength f=0.1762).

tous, while **GIC→L** transitions start giving some contributions from energies greater than ∼4.3 eV. **L→GIC** excitations occur only sporadically giving small contributions, starting from excited state $\boldsymbol{n}$=170 at 5.60 eV with the $|227\rangle \rightarrow |254\rangle$ transition. **L→L** excitations appear to be even rarer in this range of energies, starting with state $\boldsymbol{n}$=144 at 5.44 eV receiving some very small contribution from $|228\rangle \rightarrow |262\rangle$ transition.

It is also worth noticing that the first transition of triphenylphosphine (pictured in Fig. S2 at 5.23 eV, corresponding to λ =237 nm) cannot be traced back into the complex structure of the **GIC+L** model. In particular, none of the orbitals involved in transitions near 5.23 eV energy of the **GIC+L** model are localized on the ligand. In fact, as stated above, only transition $\boldsymbol{n}$=144 (0.2 eV higher than the optical gap of triphenylphosphine) of the **GIC+L** model shows some **L→L** character, but even in this case the shape of the involved orbitals (*viz.* orbitals 228 and 262, pictured in Figures S5 and S4, respectively) are very different from those reported in Fig. S3 for HOMO and LUMO+1 of the isolated ligand.

Thus, while the electronic structure of the ligand has only minor effects on the global shape of the optical spectrum of the NC (at least for energies ≤5.8 eV), the former is severely affected and reshaped by the gold core.

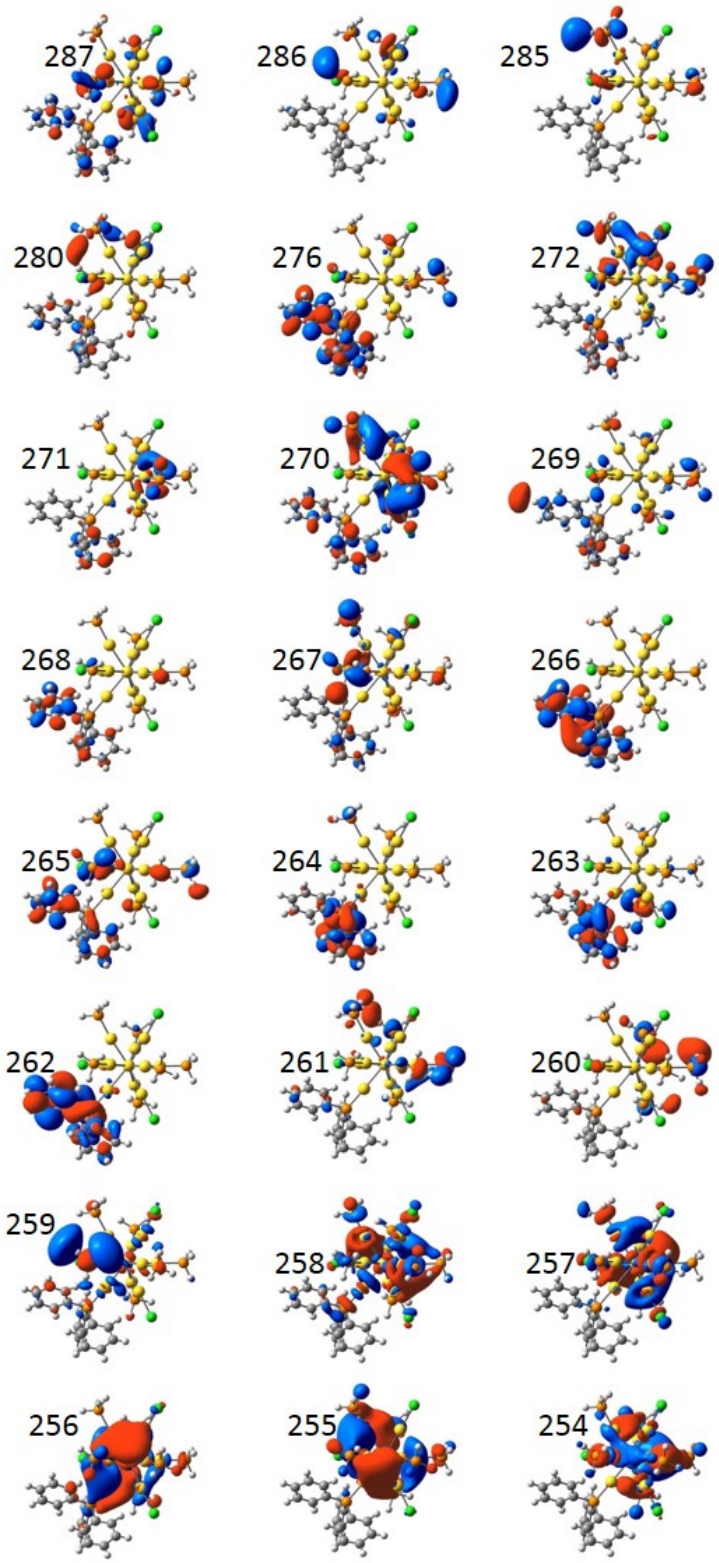

Figure S4: Contour levels of 24 **virtual** orbitals of the **GIC+L** model, at the cam-B3LYP/6-31++G level of theory Orbital 254 is the LUMO (lower right).

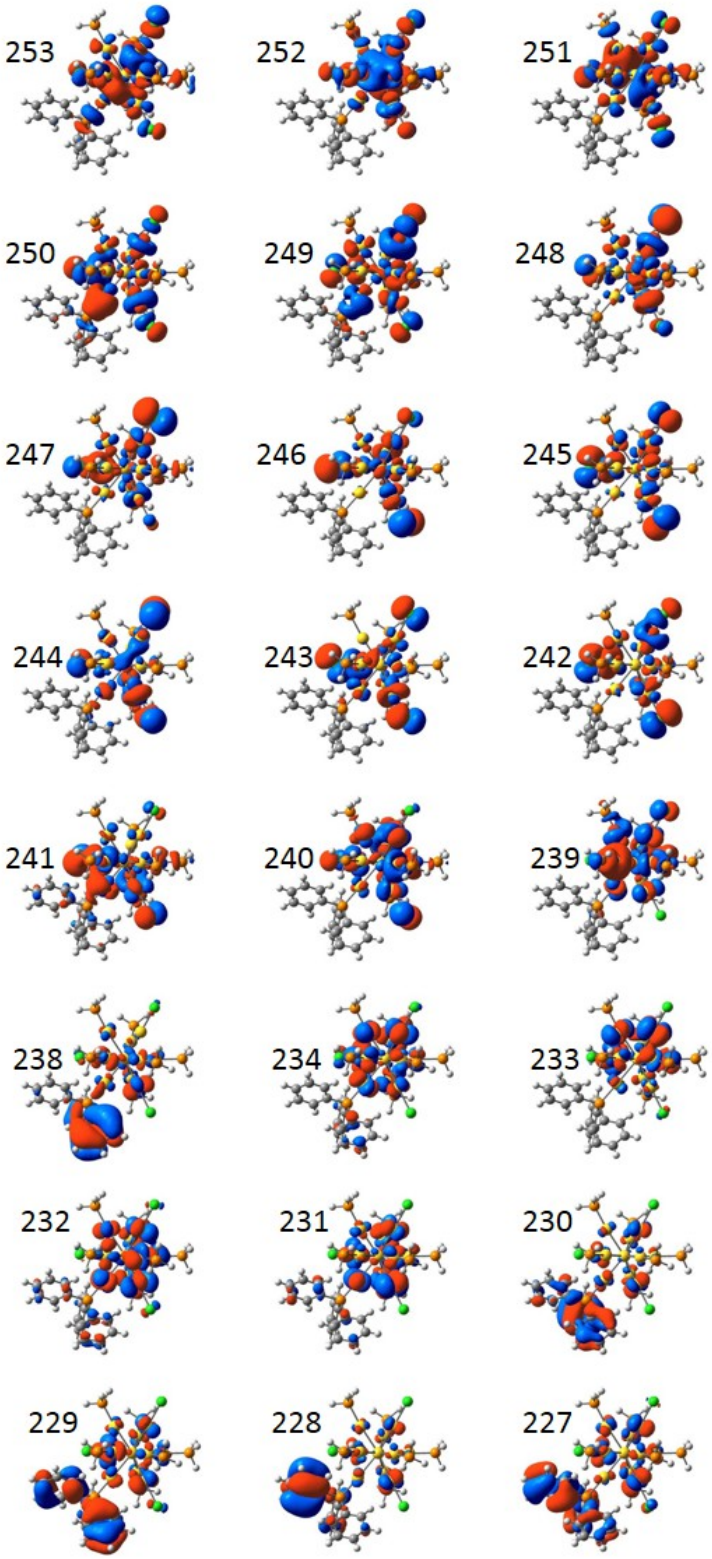

Figure S5: Contour levels of 24 **occupied** orbitals of the **GIC+L** model, at the cam-B3LYP/6-31++G level of theory. Orbital 253 is the HOMO (upper left).

Table S1: Pairs of orbitals giving contributions to 45 selected optical $S_0 \rightarrow S_n$ transitions of the GIC+L model. The leftmost column indicates the number of the transition (n). The 2nd and 3rd columns are the pairs of occupied and virtual orbitals involved into the transitions, respectively. The 4th column shows the relative contribution (CI coefficient) of the specific pair of orbitals to the transition. Contributions are ordered in decreasing absolute value. Oscillator strengths of the transitions multiplied by a 10^4 factor (5th column), their energies (6th column), and their corresponding wavelengths (7th column) are reported. Only transitions with oscillator strengths$\geq 250 \cdot 10^{-4}$ have been reported, except for the first one and n=144, which are reported due to their relevance. Transitions marked with symbol * are also (partially) reported inside the paper. Orbital 253 and 254 are the HOMO and LUMO, respectively. Calculations are performed on the GIC+L model at the cam-B3LYP/6-31++G level of theory.

n	$\langle$In. orb.$\|$	$\rightarrow$	$\|$Fin. orb.$\rangle$	CI coeff.	Osc. str.	En./eV	λ/nm
1*	253		254	0.65	41	2.91	426
1	252		254	0.15			
1	253		258	0.12			
3	252		254	0.57	268	2.99	415
3	253		256	0.26			
3	251		255	0.17			
3	251		254	-0.14			
3	253		254	-0.12			
9	251		255	0.38	504	3.23	384
9	253		257	0.28			
9	251		257	-0.25			
9	253		256	0.22			
9	253		258	-0.20			
9	252		254	-0.18			
9	252		258	-0.12			
9	251		258	-0.12			
13*	251		257	0.34	1971	3.48	357
13	253		258	0.28			
13	251		255	0.28			
13	253		256	0.23			
13	252		258	0.21			
13	252		254	-0.19			
13	252		259	0.12			
14*	251		258	0.46	1713	3.57	347
14	252		257	0.27			
14	253		257	0.21			
14	251		259	0.17			
14	250		257	-0.13			
14	252		255	0.13			
14	252		258	0.11			
15*	253		258	0.42	2903	3.58	346
15	251		257	-0.39			
15	252		256	-0.20			
15	253		259	0.15			
15	250		258	-0.14			
31	247		254	0.27	282	4.33	287
31	253		259	0.21			
31	251		259	0.19			
31	249		256	0.14			
31	253		262	0.14			
31	251		261	0.13			

n	$\langle$In. orb.$\|$	$\rightarrow$	$\|$Fin. orb.$\rangle$	CI coeff.	Osc. str.	En./eV	λ/nm
31	251		270	-0.13			
31	246		254	0.12			
31	250		257	-0.12			
31	251		271	0.12			
31	251		258	-0.12			
31	251		260	-0.11			
31	251		263	0.10			
31	251		271	0.12			
31	251		258	-0.12			
31	251		260	-0.11			
31	251		263	0.10			
33	253		263	0.24	739	4.37	284
33	253		261	0.18			
33	253		272	0.18			
33	253		262	-0.17			
33	247		255	0.15			
33	251		259	0.14			
33	253		271	0.14			
33	249		256	-0.13			
33	250		257	-0.13			
33	249		255	0.12			
33	251		262	0.11			
33	250		258	-0.11			
33	253		260	-0.10			
39	250		257	0.30	706	4.44	279
39	248		256	-0.26			
39	249		257	-0.20			
39	247		256	0.17			
39	250		258	-0.15			
39	245		254	0.12			
39	246		256	0.11			
39	252		261	0.11			
40*	250		257	0.29	1436	4.46	278
40	249		255	0.20			
40	249		257	0.20			
40	250		258	0.17			
40	247		256	0.15			
40	247		258	-0.13			
40	245		256	-0.12			
40	248		257	0.11			
40	253		261	-0.11			
41	250		258	0.29	1250	4.46	278
41	248		257	-0.19			
41	248		256	-0.19			
41	246		255	0.15			
41	245		256	0.14			
41	245		255	0.13			
41	247		256	0.11			
41	245		254	0.11			
41	249		257	-0.10			
41	250		259	0.10			

n	$\langle$In. orb.$\|$	$\rightarrow$	$\|$Fin. orb.$\rangle$	CI coeff.	Osc. str.	En./eV	λ/nm
41	252		260	0.10			
41	246		257	-0.10			
42	251		260	0.21	523	4.48	277
42	251		270	-0.19			
42	251		263	-0.17			
42	251		259	-0.15			
42	249		255	0.13			
42	248		258	0.12			
42	246		254	0.12			
42	245		254	0.12			
42	245		255	0.12			
42	251		272	-0.12			
42	251		267	0.11			
42	251		265	-0.11			
42	248		256	-0.11			
42	251		261	0.10			
44	247		255	0.24	275	4.50	276
44	247		256	-0.22			
44	249		258	-0.20			
44	250		258	0.19			
44	246		257	0.17			
44	248		256	-0.14			
44	246		255	-0.14			
44	247		257	-0.14			
44	252		263	-0.12			
44	248		254	0.11			
44	253		262	-0.11			
46	246		256	0.22	479	4.52	275
46	247		255	-0.21			
46	248		255	-0.20			
46	251		260	0.20			
46	251		259	0.18			
46	249		257	-0.14			
46	251		270	0.12			
46	251		263	0.12			
46	246		258	-0.11			
46	247		258	-0.11			
46	252		261	-0.11			
46	252		261	-0.11			
46	246		255	-0.10			
47	251		260	0.40	273	4.53	274
47	251		259	0.21			
47	246		256	-0.20			
47	248		257	-0.19			
47	249		257	0.19			
47	245		256	-0.10			
51	246		255	0.29	1036	4.59	270
51	249		258	-0.28			
51	246		257	-0.19			
51	248		257	0.18			
51	247		256	-0.16			

n	$\langle$In. orb.$\|$	$\rightarrow$	$\|$Fin. orb.$\rangle$	CI coeff.	Osc. str.	En./eV	λ/nm
51	247		255	-0.13			
51	248		255	0.12			
51	247		258	0.11			
56	239		255	0.40	335	4.68	265
56	241		255	-0.20			
56	240		254	-0.17			
56	246		254	-0.16			
56	246		258	-0.14			
56	252		261	-0.12			
56	246		257	0.10			
58	239		256	0.38	562	4.71	263
58	241		256	-0.19			
58	239		254	-0.16			
58	252		261	0.16			
58	245		257	0.12			
58	245		255	0.11			
58	247		254	0.11			
60	245		255	0.31	367	4.73	262
60	251		261	0.24			
60	245		256	0.21			
60	252		261	0.17			
60	239		256	-0.15			
60	247		255	-0.14			
60	247		256	-0.11			
60	253		264	-0.10			
62	252		261	0.27	275	4.76	261
62	244		254	0.21			
62	252		263	-0.21			
62	245		258	0.15			
62	251		261	-0.15			
62	239		255	0.10			
62	252		267	-0.12			
62	251		263	0.12			
62	245		255	-0.11			
62	252		270	0.11			
62	251		267	0.10			
63	244		254	0.32	379	4.77	260
63	239		256	0.22			
63	241		254	0.17			
63	251		261	0.12			
63	253		263	0.12			
63	247		257	0.11			
63	251		267	-0.11			
63	245		256	0.10			
64	243		254	0.30	578	4.79	259
64	245		257	-0.16			
64	245		256	0.15			
64	245		258	0.13			
64	252		263	0.12			
64	241		254	-0.11			
64	242		254	-0.11			

n	$\langle$In. orb.$\|$	$\rightarrow$	$\|$Fin. orb.$\rangle$	CI coeff.	Osc. str.	En./eV	λ/nm
64	251		261	0.11			
64	244		256	-0.10			
65	251		261	0.29	470	4.81	258
65	251		262	-0.27			
65	245		255	-0.17			
65	252		263	-0.16			
65	251		263	-0.15			
65	253		263	-0.15			
65	253		265	0.13			
65	251		270	0.14			
65	253		264	0.10			
66	243		254	0.20	484	4.81	258
66	244		254	0.19			
66	251		263	-0.18			
66	242		254	0.17			
66	245		257	0.14			
66	252		261	-0.13			
66	244		257	0.11			
66	245		258	0.11			
66	245		256	-0.10			
68*	253		264	0.37	701	4.83	256
68	253		265	0.26			
68	253		272	0.14			
68	251		263	0.13			
68	253		262	0.13			
68	243		254	-0.12			
68	251		262	0.12			
68	253		266	0.11			
68	253		270	0.11			
68	244		256	-0.10			
71	241		254	0.23	302	4.87	255
71	252		264	0.17			
71	241		256	-0.16			
71	244		255	0.14			
71	242		254	0.12			
71	251		262	-0.12			
71	252		262	0.12			
71	252		269	0.12			
71	239		254	0.11			
71	242		255	0.11			
71	252		265	-0.11			
75	243		255	0.22	508	4.91	252
75	240		254	0.21			
75	239		254	0.14			
75	245		256	-0.14			
75	251		267	-0.14			
75	252		267	0.14			
75	240		257	-0.13			
75	239		255	0.12			
75	243		254	-0.12			

n	$\langle$In. orb.$\|$	$\rightarrow$	$\|$Fin. orb.$\rangle$	CI coeff.	Osc. str.	En./eV	λ/nm
75	251		265	-0.12			
75	240		258	0.11			
77	244		256	0.20	587	4.92	252
77	241		256	-0.19			
77	240		256	-0.16			
77	240		257	-0.13			
77	242		256	-0.13			
77	252		262	-0.13			
77	242		255	0.12			
77	245		256	0.12			
77	251		265	0.12			
77	253		267	-0.12			
77	252		267	0.10			
77	240		254	-0.10			
77	243		256	0.10			
84	251		264	0.27	336	4.98	249
84	242		256	0.22			
84	253		265	-0.19			
84	240		255	0.15			
84	253		272	0.13			
84	253		267	-0.12			
84	242		255	0.11			
88	253		265	0.24	479	5.01	247
88	253		266	-0.21			
88	253		270	-0.17			
88	253		272	-0.15			
88	253		267	-0.13			
88	253		268	-0.12			
88	253		269	0.12			
88	251		262	-0.11			
88	251		274	0.11			
88	242		254	0.10			
88	245		257	-0.10			
88	253		274	-0.10			
92	252		267	0.24	592	5.04	246
92	242		256	-0.18			
92	239		257	0.14			
92	253		267	0.16			
92	244		258	-0.12			
92	251		265	-0.12			
92	241		255	-0.11			
92	252		265	0.11			
92	252		268	0.11			
93	242		256	0.18	718	5.05	245
93	251		267	0.17			
93	245		257	-0.16			
93	242		254	0.13			
93	244		258	-0.13			
93	251		264	-0.12			
93	253		266	0.12			
93	242		257	0.11			

n	$\langle$In. orb.$\|$	$\rightarrow$	$\|$Fin. orb.$\rangle$	CI coeff.	Osc. str.	En./eV	λ/nm
93	243		257	-0.11			
93	244		254	-0.11			
93	251		265	0.11			
95	243		257	0.19	865	5.07	244
95	251		272	-0.18			
95	251		268	0.16			
95	239		257	0.15			
95	251		265	0.15			
95	243		258	0.14			
95	245		258	0.14			
95	250		262	0.11			
95	240		255	-0.11			
95	241		255	-0.11			
95	253		272	0.11			
96	251		265	0.20	552	5.08	244
96	242		257	-0.17			
96	251		272	-0.17			
96	239		256	-0.11			
96	240		255	-0.14			
96	251		268	0.14			
96	241		256	-0.13			
96	252		267	0.13			
96	244		254	0.11			
96	252		271	0.11			
97	251		267	0.22	810	5.08	244
97	242		257	-0.18			
97	251		268	0.15			
97	251		271	0.15			
97	251		274	-0.14			
97	252		267	-0.14			
97	243		257	-0.14			
97	251		269	0.13			
97	251		270	0.13			
97	252		272	-0.13			
97	235		254	0.12			
97	252		270	-0.12			
97	251		262	0.11			
102	243		257	0.25	381	5.13	242
102	240		255	0.16			
102	242		258	0.16			
102	244		256	-0.14			
102	243		256	0.13			
102	241		256	0.12			
102	242		255	0.12			
102	244		258	-0.11			
102	250		259	0.11			
108	252		266	0.32	395	5.18	239
108	252		268	0.23			
108	252		269	-0.21			
108	252		265	-0.16			
108	252		275	0.16			

n	⟨In. orb.|	→	|Fin. orb.⟩	CI coeff.	Osc. str.	En./eV	λ/nm
108	252		274	0.14			
108	239		257	-0.13			
108	241		255	-0.13			
108	252		270	0.11			
109	235		254	0.18	334	5.19	239
109	244		257	0.17			
109	240		257	0.16			
109	244		255	0.15			
109	242		257	0.13			
109	232		254	-0.11			
109	240		258	-0.11			
111	251		266	0.22	402	5.21	238
111	250		262	-0.16			
111	233		254	0.14			
111	234		254	0.14			
111	241		257	-0.14			
111	251		268	0.14			
111	251		269	-0.13			
111	251		270	0.13			
111	252		266	0.13			
111	245		258	-0.12			
111	251		265	-0.12			
144*	253		268	0.15	158	5.44	228
144	250		259	0.15			
144	253		266	-0.14			
144	249		259	-0.13			
144	252		276	-0.13			
144	253		278	0.12			
144	253		287	0.12			
144	248		260	0.11			
144	252		273	0.11			
144	252		278	-0.11			
144	252		282	0.11			
144	228		262	0.10			
144	253		264	0.10			
170*	232		257	0.13	450	5.60	221
170	229		254	0.13			
170	232		257	0.13			
170	234		257	-0.12			
170	227		254	-0.11			
170	248		261	-0.11			
170	253		272	0.11			
170	253		276	-0.11			
170	235		258	0.10			
186	234		258	0.18	410	5.70	218
186	252		280	-0.17			
186	252		276	0.15			
186	253		285	-0.13			
186	253		287	0.12			
186	233		258	0.10			

n	$\langle$**In. orb.**$\vert$	$\rightarrow$	$\vert$**Fin. orb.**$\rangle$	**CI coeff.**	**Osc. str.**	**En./eV**	λ**/nm**
186	251		276	0.10			
188	248		259	0.15	482	5.71	217
188	248		260	0.13			
188	231		258	0.11			
188	251		274	-0.11			
188	251		280	0.11			
188	251		286	0.10			
198	239		259	0.19	283	5.77	215
198	231		257	-0.16			
198	251		280	-0.15			
198	247		259	0.13			
198	248		262	0.13			

References

(1) Muniz-Miranda, F.; Menziani, M. C.; Pedone, A. *The Journal of Physical Chemistry C* **2014**, *118*, 7532–7544.

(2) Baerends, E. J.; Gritsenko, O. V.; van Meer, R. *Phys. Chem. Chem. Phys.* **2013**, *15*, 16408–16425.

(3) Gutrath, B. S.; Englert, U.; Wang, Y.; Simon, U. *European Journal of Inorganic Chemistry* **2013**, *2013*, 2002–2006.